PHYSICAL REVIEW C **94**, 044321 (2016)

Statistical γ-decay properties of ^{64}Ni and deduced (n,γ) cross section of the s-process branch-point nucleus ^{63}Ni

L. Crespo Campo,[1,*] F. L. Bello Garrote,[1] T. K. Eriksen,[1,†] A. Görgen,[1] M. Guttormsen,[1] K. Hadynska-Klek,[1,‡] M. Klintefjord,[1] A. C. Larsen,[1] T. Renstrøm,[1] E. Sahin,[1] S. Siem,[1] A. Springer,[1,2] T. G. Tornyi,[1,3,†] and G. M. Tveten[1]

[1]*Department of Physics, University of Oslo, N-0316 Oslo, Norway*

[2]*Department of Physics, Karlsruhe Institute of Technology, D-76131 Karlsruhe, Germany*

[3]*Institute of Nuclear Research of the Hungarian Academy of Sciences (MTA Atomki), Debrecen, Hungary*

(Received 29 February 2016; revised manuscript received 4 June 2016; published 26 October 2016)

Particle-γ coincidence data have been analyzed to obtain the nuclear level density and the γ-strength function of ^{64}Ni by means of the Oslo method. The level density found in this work is in very good agreement with known energy levels at low excitation energies as well as with data deduced from particle-evaporation measurements at excitation energies above $E_x \approx 5.5$ MeV. The experimental γ-strength function presents an enhancement at γ energies below $E_\gamma \approx 3$ MeV and possibly a resonancelike structure centered at $E_\gamma \approx 9.2$ MeV. The obtained nuclear level density and γ-strength function have been used to estimate the (n,γ) cross section for the s-process branch-point nucleus ^{63}Ni, of particular interest for astrophysical calculations of elemental abundances.

DOI: 10.1103/PhysRevC.94.044321

I. INTRODUCTION

The nuclear level density and the γ-strength function[1] are two average nuclear quantities that govern the statistical γ decay of nuclei. These quantities have been studied for decades, revealing nuclear processes such as breaking of nucleon pairs [2–4] or γ resonances[2] [1,5,6]. However, as of today, many questions about these processes remain unanswered, including those regarding the origin of γ resonances or the theoretical description of nuclear level densities.

The nuclear physics group at the University of Oslo has contributed to increase the experimental data on nuclear level densities and γ-strength functions with the so-called Oslo method [7–10], which allows for the simultaneous extraction of these two properties from particle-γ coincidence measurements. One of the most surprising features observed in the γ-strength function is the increased probability of γ decay with γ energies below 2–4 MeV, first seen in ^{56,57}Fe in 2004 [11]. Since then, this low-energy enhancement or *upbend* has been measured for several nuclei from Sc to Sm [11–19] and confirmed with an independent method for ^{95}Mo [20].

The physical mechanisms underlying this enhancement are still not clarified. There is currently no consensus on whether its character is mostly of $E1$ or $M1$ nature and so far only for ^{60}Ni are there strong indications of the $M1$ character of this upbend [21]. In the last years, two main theories have been proposed. Calculations based on the quasiparticle random phase approximation (QRPA) predict an increase in the $E1$ strength at low γ energies in ^{94,96,98}Mo [22]. However, shell-model calculations indicate an $M1$ origin of this low-energy enhancement [23,24]. It must be noted that no shell-model calculations of $E1$ transitions are available in the literature at present, neither are there $M1$ strength calculations for the upbend within a QRPA approach. Further theoretical and experimental studies are therefore vital to clarify the origin of this low-energy enhancement of the γ strength. Moreover, there is currently very limited knowledge regarding the systematic evolution of the upbend with nuclear features such as mass, deformation, or number of nucleons away from closed shells. Therefore, additional experimental data on the low-energy γ strength of nuclei in the Fe-Sm region would be of great value.

The impact of the upbend and γ resonances is especially significant for nuclear astrophysics, where neutron-capture cross sections play a major role in heavy-element nucleosynthesis calculations and determination of elemental abundances. The nuclear level density and the γ-strength function can be used to estimate (n,γ) cross sections, which can be highly increased by the presence of γ resonances and the low-energy enhancement of the γ strength [25,26]. This becomes of particular interest in the cases where neutron capture cross-section data are either not available or limited to a narrow energy range, as it is often the case for s-process branch-point nuclei [27]. In this respect, the study of ^{64}Ni is especially interesting, because in this case two recent direct measurements of the (n,γ) cross section exist [28,29]. These direct measurements can therefore be compared to the estimates based on the nuclear level density and the γ-strength functions obtained with the Oslo method, providing an excellent benchmark for our approach.

In this work, the γ-strength function and level density of ^{64}Ni will be presented, obtained through the Oslo method from the study of the ^{64}Ni$(p,p'\gamma)^{64}$Ni reaction. Special attention will be paid to the γ-strength function, in particular the upbend and the possible presence of a resonancelike structure at ≈9.2 MeV. In addition, the results will be used to estimate the neutron capture cross section and reaction rate in ^{63}Ni, an s-process branch-point nucleus relevant in nuclear

*l.c.campo@fys.uio.no
†Current address: Department of Nuclear Physics, Research School of Physics and Engineering, The Australian National University, ACTON, ACT 2601, Australia.
‡Current address: Istituto Nazionale di Fisica Nucleare, Laboratori Nazionali di Legnaro, 2 35020 Legnaro (Padua), Italy.

[1]Average reduced γ-transition probability [1].

[2]Resonances in γ absorption and emission.

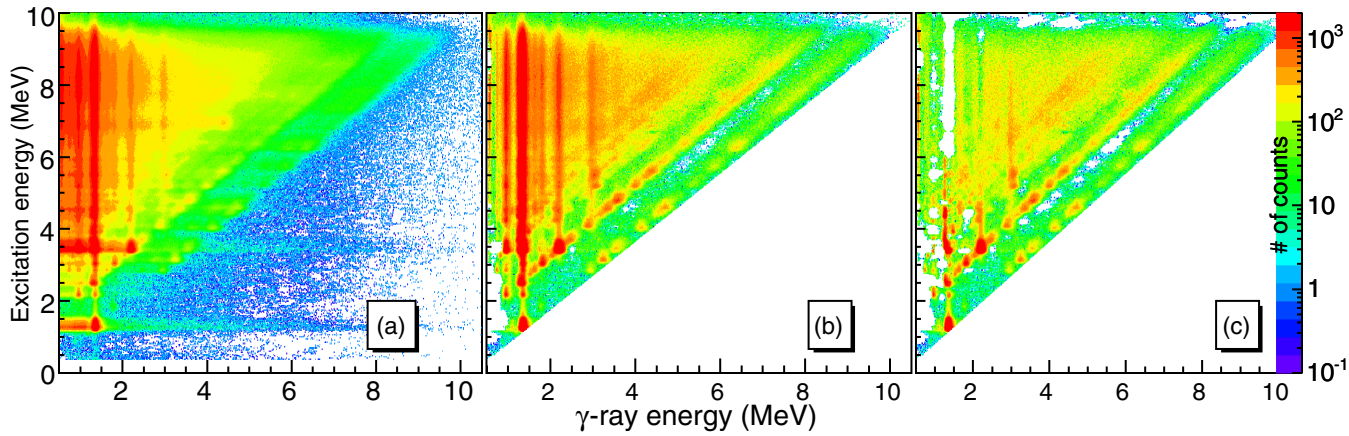

FIG. 1. Original (a), unfolded (b), and first-generation (c) coincidence matrices for ^{64}Ni from the ^{64}Ni$(p,p'\gamma)^{64}$Ni reaction. The x axis represents the γ energy, while the y axis gives the excitation energy of ^{64}Ni. The number of counts is represented by the color scale.

astrophysics [30]. Finally, the results will be discussed and compared to theoretical calculations and experimental data.

This article is organized as follows. In Sec. II the experimental details and data analysis are summarized. In Sec. III the normalization procedure of the level density and γ-strength function is discussed. Further, in Sec. IV the obtained results are used to estimate the ^{63}Ni$(n,\gamma)^{64}$Ni cross section and reaction rate with the code TALYS [31] and compared with other experimental data and models. Finally, a summary and outlook are given in Sec. V.

II. EXPERIMENTAL DETAILS AND DATA ANALYSIS

The experiment was performed at the Oslo Cyclotron Laboratory (OCL) using a 99% enriched ^{64}Ni self-supporting target of 1 mg/cm^2 thickness. A 16-MeV proton beam was used to study the ^{64}Ni$(p,p'\gamma)^{64}$Ni reaction, running for 5 days with typical beam currents of 0.2–0.4 nA.

Particle-γ coincidences were measured with the silicon ring (SiRi) particle-detector system [32] and the CACTUS γ-detection array [33]. The SiRi system consists of eight telescope ΔE-E silicon detectors, each of them formed by a 130-μm thin layer located in front of a 1550-μm-thick back detector. Each of the thin detectors is divided into eight strips, where one strip has an angular resolution of $\Delta\theta = 2^\circ$. In total, the SiRi system contains 64 individual detectors, with a solid-angle coverage of ≈6%. For this experiment, the SiRi detector system was placed in backward angles with respect to the beam direction, covering scattering angles from 126° to 140° in the laboratory frame.

TABLE I. γ-ray transitions used to measure the response functions of CACTUS detectors.

E_γ (keV)	E_x (keV)	Nucleus
847	847	^{56}Fe
1238	2085	^{56}Fe
1779	1779	^{28}Si
2839	4618	^{28}Si
3089	3089	^{13}C
4497	6276	^{28}Si
6130	6130	^{16}O
9925	9929	^{28}Si

The CACTUS array consists of 26 collimated 5 × 5-inch NaI(Tl) crystals. The total efficiency of CACTUS is 14.1(1)% at $E_\gamma = 1332.5$ keV. The charged ejectiles and the γ rays were measured in coincidence event by event, with a time resolution (full width at half maximum) of ≈15 ns.

By measuring the energy deposited by the ejected particles in the thin (ΔE) and thick (E) detectors, ΔE-E curves were obtained allowing for the identification of the different charged-particle species. In this case the gate was set on the ejected protons to select the $(p,p'\gamma)$ reaction channel. From reaction kinematics, the measured energies of the ejected particles were used to obtain the corresponding excitation energy of the residual nucleus.

As a result, the excitation energy of ^{64}Ni vs coincident γ rays (the coincidence matrix) was obtained, as shown in Fig. 1(a). The γ-ray spectra were then unfolded for each excitation-energy bin (corrected for the response of the detectors in CACTUS), as described in Ref. [7]. The applied response functions and detector efficiencies were obtained in 2012 from in-beam γ lines listed in Table I. The (p,p') reaction was used in all cases except for ^{13}C, for which the stripping reaction ^{12}C$(d,p)^{13}$C was utilized [13]. With this unfolding method, no artificial fluctuations are introduced and the experimental statistical uncertainties are preserved. Figure 1(b) shows the unfolded matrix for ^{64}Ni, in which several discrete peaks at $E_x \leqslant 4$ MeV are clearly visible.

From the unfolded γ spectra, the distribution of first-generation (primary) γ rays[3] for each excitation-energy bin was extracted via an iterative subtraction technique [8]. The basic assumption of this method is that the decay routes are the same regardless of whether the initial states were populated directly via the nuclear reaction or from γ decay from above-lying states. For a more detailed discussion of the

[3]The first γ ray emitted in the decay cascade.

possible errors and uncertainties of this method, see Ref. [10]. The first-generation matrix for ^{64}Ni can be seen in Fig. 1(c).

From the first-generation matrix, the functional form of the level density and the γ-transmission coefficient was obtained with an iterative subtraction method described in Ref. [9]. In this procedure, one assumes that the reaction leads to a compound nucleus which decays independently of how it was formed, i.e., a statistical decay process [34]. One can then assume that the relation

$$P(E_\gamma, E_x) \propto \rho(E_f)\mathcal{T}(E_\gamma) \tag{1}$$

holds, where $P(E_\gamma, E_x)$ is the experimental first-generation matrix as a function of the γ energy E_γ and the initial excitation energy of the nucleus E_x, $\rho(E_f)$ is the level density at the final excitation energy E_f, with $E_f = E_x - E_\gamma$, and $\mathcal{T}(E_\gamma)$ is the γ-transmission coefficient. With every point of the ρ and $\mathcal{T}$ functions as an independent variable, the least-χ^2 fit of $\rho\mathcal{T}$ is calculated, reaching a global minimum within 10–20 iterations. It is important to note that no additional assumptions are made for the functional form of ρ and $\mathcal{T}$ in the least-χ^2 fit.

As seen in Eq. (1), the γ-transmission coefficient $\mathcal{T}$ is a function of E_γ only. This is based on the generalized Brink hypothesis [35], which states that any collective decay mode has the same properties whether it is built on the ground state or on excited states. The Brink hypothesis has been proven incorrect for nuclear reactions involving high temperatures and/or spins [36]. However, in the present work the reached spin range and temperature are rather low, so it is reasonable to assume that the Brink hypothesis holds, as demonstrated in Refs. [11,15,37].

To ensure that the decay from compound-nucleus states is dominant and the hypothesis of statistical decay holds, a section of the first-generation coincidence matrix must be selected. In the present work, a minimum excitation energy $E_{x,\mathrm{low}} = 5.82$ MeV was chosen together with a lower limit in the γ energy of $E_{\gamma,\mathrm{low}} = 1.98$ MeV. In addition, to exclude data corresponding to the γ decay of ^{63}Ni, one has to ensure that the neutron emission channel in ^{64}Ni is not included. Therefore, an upper limit in the excitation energy $E_{x,\mathrm{up}} = 9.66$ MeV was employed, below the sum of the neutron separation energy in ^{64}Ni, $S_n = 9.658$ MeV, and the energy of the first excited state in ^{63}Ni at 0.087 MeV [38].

The result of the least-χ^2 fit is the functional form of ρ and $\mathcal{T}$. In particular, if $\rho(E_x - E_\gamma)$ and $\mathcal{T}(E_\gamma)$ are the solutions of a fit to a given set of experimental data, it can be proven [9] that the transformations $\tilde{\rho}(E_x - E_\gamma)$ and $\tilde{\mathcal{T}}(E_\gamma)$ would give identical fits, where

$$\tilde{\rho}(E_x - E_\gamma) = \mathscr{A}\exp[\alpha(E_x - E_\gamma)]\,\rho(E_x - E_\gamma), \tag{2}$$

$$\tilde{\mathcal{T}}(E_\gamma) = \mathscr{B}\exp(\alpha E_\gamma)\mathcal{T}(E_\gamma). \tag{3}$$

Therefore, to get the physical solution, the transformation parameters $\mathscr{A}$, α, and $\mathscr{B}$ were determined from experimental data in a normalization procedure. Finally, once the γ-transmission coefficient $\mathcal{T}(E_\gamma)$ was determined, the γ-strength function $f_L(E_\gamma)$ was obtained with the relation [39,40],

$$f_L(E_\gamma) = \frac{\mathcal{T}(E_\gamma)}{2\pi E_\gamma^{2L+1}}, \tag{4}$$

where L is the multipolarity of the transition. Generally, it is seen that the main contribution to the experimental $\mathcal{T}(E_\gamma)$ is from dipole radiation ($L = 1$) [13,40].

III. NORMALIZATION OF THE LEVEL DENSITY AND THE γ-STRENGTH FUNCTION

A. Level density

To normalize the nuclear level density, discrete energy levels [38] were used at low excitation energies together with an estimated value of the level density at the neutron separation energy, $\rho(S_n)$. Because the level scheme for ^{64}Ni is regarded to be complete up to 4.762 MeV [41], the normalization was performed requiring a good agreement with discrete energy levels below $E_x \approx 4.76$ MeV. For the estimation of $\rho(S_n)$, an expression is usually applied [39],

$$\rho(S_n) = \frac{2\sigma^2}{D_0}\frac{1}{(I_t+1)\exp[-(I_t+1)^2/2\sigma^2] + I_t\exp\left[-I_t^2/2\sigma^2\right]}, \tag{5}$$

where D_0 is the level spacing of s-wave *resonances*, σ is the spin cutoff parameter, and I_t is the ground-state spin of the target nucleus in the (n,γ) reaction ($1/2^-$ for ^{63}Ni). Notice that Eq. (5) is obtained when the following spin distribution $g(E_x, I)$ is assumed [2,3],

$$g(E_x, I) \simeq \frac{2I+1}{2\sigma^2}\exp[-(I+1/2)^2/2\sigma^2], \tag{6}$$

for a specific excitation energy E_x, spin I, and a spin cutoff parameter σ. Because no tabulated values of D_0 were available for ^{64}Ni, its $\rho(S_n)$ was obtained from systematics of the Ni isotopes for which a D_0 value was available [41,42]. The value of σ was found for each of the Ni isotopes and used together with its tabulated D_0 value to estimate $\rho(S_n)$ by means of Eq. (5). The resulting $\rho(S_n)$ values were then fitted to an exponential function by means of a χ^2-minimization routine, leading to the estimation of $\rho(S_n)$ for ^{64}Ni together with its uncertainty. From the resulting value of $\rho(S_n)$, the corresponding D_0 value was then obtained by means of Eq. (5).

In this work, two different models for the spin cutoff parameter have been applied. First, the $\rho(S_n)$ values for the Ni isotopes were obtained with σ given by the backshifted Fermi gas (BSFG) model from global systematics of Ref. [43],

$$\sigma^2(E_x) = 0.391A^{0.675}(E_x - 0.5\,\mathrm{Pa}')^{0.312}, \tag{7}$$

where A is the mass number of the nucleus and Pa′ is the deuteron pairing energy. As a result, a value $\rho^{\S}(S_n) = 2620(890)$ MeV^{-1} was obtained for the level density of ^{64}Ni, with $S_n = 9.658$ MeV. In addition, the procedure was repeated using the values of σ given by the rigid moment of inertia

TABLE II. Parameters used for the calculation of $\rho(S_n)$ for ^{64}Ni (see text).

Nucleus	I_t^π	D_0 (10^3 eV)	S_n (MeV)	a[a] (MeV^{-1})	E_1[a] (MeV)	σ[a] (S_n)	ρ[a] (S_n) (10^3 MeV^{-1})	a[b] (MeV^{-1})	E_1[b] (MeV)	σ[b] (S_n)	ρ[b] (S_n) (10^3 MeV^{-1})
^{59}Ni	0^+	13.4(9)	8.999	5.76	−0.14	3.47	1.87(13)	6.11	−0.26	4.14	2.64(18)
^{60}Ni	$3/2^-$	2.0(7)	11.388	6.16	1.19	3.56	3.80(130)	6.57	1.12	4.22	5.09(180)
^{61}Ni	0^+	13.8(9)	7.82	6.64	−0.22	3.44	1.79(12)	6.97	−0.38	4.00	2.39(16)
^{62}Ni	$3/2^-$	2.10(15)	10.60	6.95	1.22	3.55	3.61(26)	7.32	1.13	4.08	4.55(33)
^{63}Ni	0^+	16.0(30)	6.838	7.40	−0.17	3.4	1.51(28)	7.68	−0.38	3.89	1.95(37)
^{65}Ni	0^+	23.6(30)	6.098	8.00	−0.11	3.37	1.01(13)	8.24	−0.39	3.82	1.28(16)

[a]Systematics and σ model based on Egidy and Bucurescu [43].
[b]Systematics and σ model based on Egidy and Bucurescu [44].

(RMI) model from Ref. [44],

$$\sigma^2(E_x) = 0.0146A^{5/3}\frac{1+\sqrt{1+4a(E_x-E_1)}}{2a}, \quad (8)$$

were a and E_1 are the level density and shift parameters in the BSFG model obtained from global systematics of Ref. [44]. A new value $\rho^{\ddagger}(S_n) = 3470(1180)$ MeV^{-1} was then obtained. A summary of the values used to estimate $\rho(S_n)$ for ^{64}Ni is shown in Table II. The resulting values of $\rho(S_n)$ and D_0 for ^{64}Ni are included in Table III.

With the Oslo method, the nuclear level density is extracted only up to $E_x \approx S_n - E_{\gamma,\mathrm{low}}$. To normalize to the value of the level density at the neutron separation energy, an interpolation between our data and $\rho(S_n)$ was applied using the constant-temperature model (CTM), which expresses the nuclear level density as [2,45]

$$\rho(E_x) = \frac{1}{T}\exp\frac{E_x - E_0}{T}, \quad (9)$$

where E_0 is the energy backshift and T is the nuclear temperature parameter. A summary of the parameters used for the normalization of the level density and the resulting values of $\rho(S_n)$ is shown in Table III. The parameters E_0 and T were chosen so as to achieve a good agreement between the level density obtained in this work at $E_x \approx 4.76$ MeV and the estimated value of $\rho(S_n)$. The normalization procedure was performed using the two different models of the spin cutoff parameter given by Eqs. (7) and (8), taking into account the estimated uncertainties for $\rho(S_n)$ in each case.

The normalized level densities for ^{64}Ni are depicted in Fig. 2 for both the value of σ obtained from Eq. (7) (normalization 1) and the value obtained from Eq. (8) (normalization 2). In addition, estimates of the upper and lower limits for the level density have been included, corresponding to the maximum and minimum values of $\rho(S_n)$ given by $\rho^{\ddagger}(S_n)$ and $\rho^{\S}(S_n)$ plus/minus their respective uncertainties. The resulting level densities from normalizations 1 and 2 are very similar, with the estimated values of $\rho(S_n)$ and the temperature parameter T in good agreement, as seen in Table III. The experimental data for the level density reproduce satisfactorily the discrete energy levels at low excitation energy, where both the ground state and the first excited 2^+ state at 1.345 MeV are clearly seen [38]. As seen in Fig. 1(c), the strong diagonal going through $E_x = E_\gamma + 1.345$ MeV indicates that the 2^+ state is strongly populated in γ decays following the inelastic proton scattering studied in this work. This results in the bigger area of the peak for the 2^+ first excited state with respect to the ground state shown in Fig. 2. At excitation energies above $E_x \approx 4.5$ MeV a saturation of known energy levels is observed. Above $E_x \approx 5$ MeV the level density seems to be well described by the CTM [2,45], as previously seen for other nuclei such as ^{50,51}V [17] or ^{97}Mo [46].

As a final remark in this section, it must be noted that in Eq. (5) it is assumed that both parities contribute equally to the level density at S_n (see Refs. [9,10]). This is in agreement with the experimental observations for nuclei such as ^{58}Ni, for which the effect of parity asymmetry in the level density is seen to be small at the neutron separation energy (S_n = 12.216 MeV) and down to excitation energies of $E_\gamma \approx 8.5$ MeV [47]. However, one can try to estimate the effect of the parity distribution in ^{64}Ni by including the parity asymmetry coefficient ζ in our expressions, given by [48]

$$\zeta = \frac{\rho_+ - \rho_-}{\rho_+ + \rho_-}, \quad (10)$$

where ρ_+ and ρ_- are the positive- and negative-parity level densities. The level density can then be expressed as a function of energy, spin, and parity [49] as

$$\rho_\alpha(E_x, I, \pi) = \rho(E_x)g(E_x, I)\mathscr{P}(E_x, \pi), \quad (11)$$

where $\rho(E_x)$ is the total level density at the excitation energy E_x, $g(E_x, I)$ is the spin distribution, and $\mathscr{P}(E_x, \pi)$ is the parity

TABLE III. Parameters used to normalize the level density of ^{64}Ni (see text).

Model for σ	$\sigma(S_n)$	D_0 (10^3 eV)	T (MeV)	E_0 (MeV)	$\rho(S_n)$ (10^3 MeV^{-1})	$\rho_\zeta(S_n)$ (10^3 MeV^{-1})
BSFG (2009)	3.52[a]	$5.06^{+2.64}_{-1.26}$	1.13(0.13)[a]	0.63(0.87)[a]	2.62(89)[a]	2.91(98)[a]
RMI (2006)	4.05[a]	$5.00^{+2.55}_{-1.30}$	1.07(0.11)[a]	0.86(0.54)[a]	3.47(118)[a]	3.85(131)[a]

[a]Estimated from systematics.

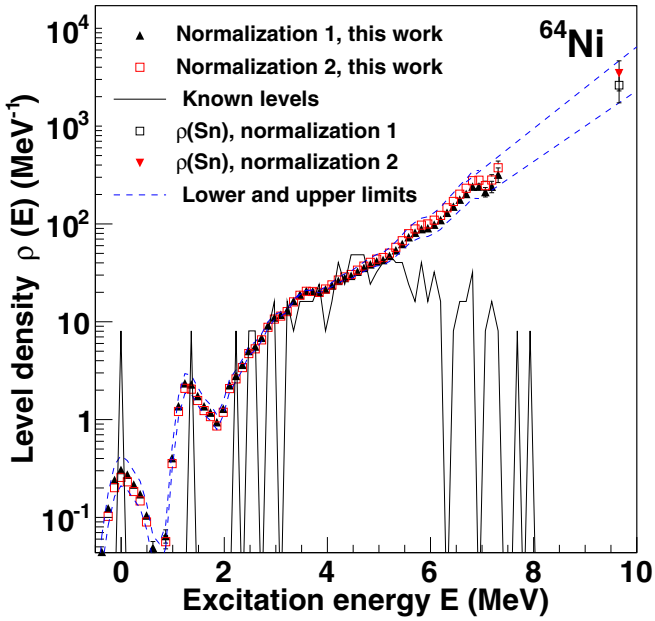

FIG. 2. Level density for ^{64}Ni as obtained in two different normalizations. Normalization 1 (see text) corresponds to a spin cutoff parameter σ within the model of Ref. [43], while in normalization 2 the model of Ref. [44] has been applied. For both normalizations, discrete energy levels have been used at low energies and a value of $\rho(S_n)$ has been obtained corresponding to the considered model for σ. The constant temperature model has been used for interpolation between the experimental data and the point $\rho(S_n)$ in each case. The bin width is 124 keV.

projection factor. Defining these projectors for both positive and negative parities,

$$\mathscr{P}_+ = \mathscr{P}(E_x,\pi_+) = \frac{\rho_+}{\rho} = \frac{1+\zeta}{2}, \tag{12}$$

$$\mathscr{P}_- = \mathscr{P}(E_x,\pi_-) = \frac{\rho_-}{\rho} = \frac{1-\zeta}{2}, \tag{13}$$

and keeping in mind that

$$\mathscr{P}_+ + \mathscr{P}_- = 1, \tag{14}$$

one can get an expression for the neutron resonance spacing at S_n, reaching states of parity $\pi_f = \pi(-1)^l$, where l is the neutron orbital angular momentum number, while π and π_f are the parities of the target and the resonance state, respectively. More specifically, for s-wave neutrons, $l = 0$, leading to [10]

$$\frac{1}{D_0} = \rho(S_n)\mathscr{P}(S_n,\pi)\left[g\left(S_n, J = I_t + \frac{1}{2}\right) + g\left(S_n, J = I_t - \frac{1}{2}\right)\right]. \tag{15}$$

Equation (15) can be then expressed as

$$\frac{1}{D_0} = \rho(S_n)\frac{1\pm\zeta}{2}\left[g\left(S_n, I = I_t + \frac{1}{2}\right) + g\left(S_n, I = I_t - \frac{1}{2}\right)\right], \tag{16}$$

where I_t is the spin of the target nucleus and the + or − sign are used depending on the positive or negative parity of the ground state. Therefore, the final expression obtained for $\rho(S_n)$ in ^{64}Ni with parity asymmetry is

$$\rho_\zeta(S_n) = \frac{2\sigma^2}{D_0(1-\zeta)}\frac{1}{(I_t+1)\exp\left[-\frac{(I_t+1)^2}{2\sigma^2}\right] + I_t\exp\left[-\frac{(I_t)^2}{2\sigma^2}\right]}. \tag{17}$$

Using the microscopic calculations from Ref. [50], a parity asymmetry $\zeta \simeq 0.1$ at $E_x = S_n$ was found. Including this parity asymmetry, new values for the level density at $E_x = S_n$ were obtained for both models of σ, shown in Table III as $\rho_\zeta(S_n)$. The estimated values of $\rho_\zeta(S_n)$ are within the error bars of $\rho(S_n)$, without parity asymmetry. The inclusion of parity asymmetry on ^{64}Ni results in a value $\rho_\zeta(S_n)$ which is ≈11% higher than the value of $\rho(S_n)$, for which the systematic uncertainty is ≈34%. Therefore, the estimated $\rho(S_n) = 2620(890)$ MeV^{-1} using $\sigma = 3.52$ and assuming parity symmetry can be considered our lower limit for the level density at $E_x = S_n$, while the value with $\sigma = 4.05$ and $\zeta \simeq 0.1$, $\rho_\zeta = 3850(1310)$ MeV^{-1}, can be considered our estimated upper limit. Again, see Ref. [10] for more details on the systematic errors of the normalization procedure.

B. γ-strength function

In previous works where the Oslo method was applied, the normalization of the γ-strength function was often done by using the relationship between the average, total radiative width at S_n, $\langle\Gamma_{\gamma,0}\rangle$, and the γ-transmission coefficient, $\mathscr{T}(E_\gamma)$, where the values of $\langle\Gamma_{\gamma,0}\rangle$ can be obtained from s-wave neutron resonances [39].

In our case, no experimental value for the $\langle\Gamma_{\gamma,0}\rangle$ parameter was available for ^{64}Ni. The determination of this parameter from systematics of other Ni isotopes was difficult, because the tabulated values for $\langle\Gamma_{\gamma,0}\rangle$ had very large uncertainties (up to 50% in some cases) [41]. Moreover, in the mass region considered in this work, big differences in the $\langle\Gamma_{\gamma,0}\rangle$ values are often seen between isotopes of similar mass. Therefore, to normalize the γ-strength function of ^{64}Ni, photoneutron cross-section measurements were used to extract the γ-strength function of ^{60}Ni [51] and ^{66}Zn [52] at the giant dipole resonance (GDR) via the relationship

$$f(E_\gamma) = \frac{1}{3\pi^2\hbar^2c^2}\frac{\sigma(E_\gamma)}{E_\gamma}, \tag{18}$$

where $\sigma(E_\gamma)$ is the photoneutron cross section, while the factor $(3\pi^2\hbar^2c^2)^{-1} = 8.674\times10^{-8}$ mb^{-1} MeV^{-2} gives the conversion to units of MeV^{-3} [39].

The GDR data were then used to estimate the $E1$ γ strength in ^{64}Ni associated with the low-energy tail of the GDR. This estimation was possible because the GDR strength has been seen to vary slowly within isotopes and neighboring nuclei given that the nuclear deformation is similar. This is reflected in the Thomas-Reiche-Kuhn (TRK) sum rule, which relates the energy-weighted $E1$ summed strength to the atomic and mass numbers of the nucleus [53]. The application of the TRK sum rule gives values of 896, 945, and 988 mb MeV for ^{60}Ni, ^{64}Ni,

and ^{66}Zn, respectively, indicating that the summed $E1$ strength for ^{64}Ni should be somewhere in between the estimates for ^{60}Ni and ^{66}Zn, closer to ^{66}Zn. These nuclei should have a similar deformation [38] and it is therefore reasonable to believe that the low-energy tail of the GDR for ^{64}Ni should be, at least to a great extent, very similar to that for ^{60}Ni and ^{66}Zn.

The experimental data on ^{60}Ni and ^{66}Zn were used to obtain an estimate of the GDR parameters and their uncertainties within a generalized Lorentzian (GLO) model [39]. For this estimation both data sets were used, with more weight on the ^{66}Zn data for the reasons discussed above. The GLO model expresses the $E1$ GDR strength f_{E1}^{GLO} as

$$f_{E1}^{\mathrm{GLO}}(E_\gamma) = \frac{\sigma_{E1}\Gamma_{E1}}{3\pi^2\hbar^2c^2}\left[\frac{E_\gamma\Gamma_K}{\left(E_\gamma^2 - E_{E1}^2\right)^2 + E_\gamma^2\Gamma_K^2} + 0.7\frac{\Gamma_{K,0}}{E_{E1}^3}\right], \tag{19}$$

where σ_{E1}, E_{E1}, and Γ_{E1} are the peak cross section, energy centroid, and resonance width parameters, respectively. Here, Γ_K is a function of the γ energy E_γ and the nuclear temperature parameter T_f given by

$$\Gamma_K(E_\gamma, T_f) = \frac{\Gamma_{E1}}{E_{E1}^2}\left(E_\gamma^2 + 4\pi^2T_f^2\right), \tag{20}$$

where the value of $\Gamma_K(0, T_f)$ is expressed as $\Gamma_{K,0}$ in Eq. (19). For deformed nuclei, the GDR strength is defined as the sum of two components, each of them given by Eq. (19). Therefore, the GDR parameters that needed to be determined were T_f, $E_{E1,i}$, $\Gamma_{E1,i}$, and $\sigma_{E1,i}$, where $i = 1,2$ indicates whether the oscillation is parallel or perpendicular to the main symmetry axis. From the resulting estimates of the GDR strength in ^{64}Ni, the absolute normalization for the γ-strength function was obtained. Taking into account the uncertainties in the GDR parameters, upper and lower limits for the γ-strength function could be estimated.

Figure 3 shows the γ-strength function of ^{64}Ni obtained in this work (black squares), together with the estimated lower and upper limits (solid green lines). In addition, the ^{60}Ni and ^{66}Zn GDR data used for normalization have been included. The estimated GDR strength for ^{64}Ni within a GLO model (blue line) is depicted for the ^{64}Ni data shown as black squares. Data on the GDR of ^{68}Ni [54] has also been included in Fig. 3, showing a good agreement with the upper limit for the γ-strength function of ^{64}Ni.

As seen from Fig. 3, the experimental data on ^{64}Ni suggest the presence of additional strength compared to the tail of the GDR. In particular, the results indicate a low-energy enhancement below 3 MeV (upbend), which can be reproduced if an additional term f^{upb} is included in the strength:

$$f^{\mathrm{upb}} = \frac{1}{3\pi^2\hbar^2c^2}CE_\gamma^{-\eta}. \tag{21}$$

In addition, depending on the normalization of the γ strength, the data suggest an enhancement with respect to the GLO strength that can be described with a resonancelike term centered at $E_\gamma \approx 9.2$ MeV. This is the case for the ^{64}Ni data depicted as black squares in Fig. 3, which cannot be reproduced solely with the GLO and upbend terms. To account for this

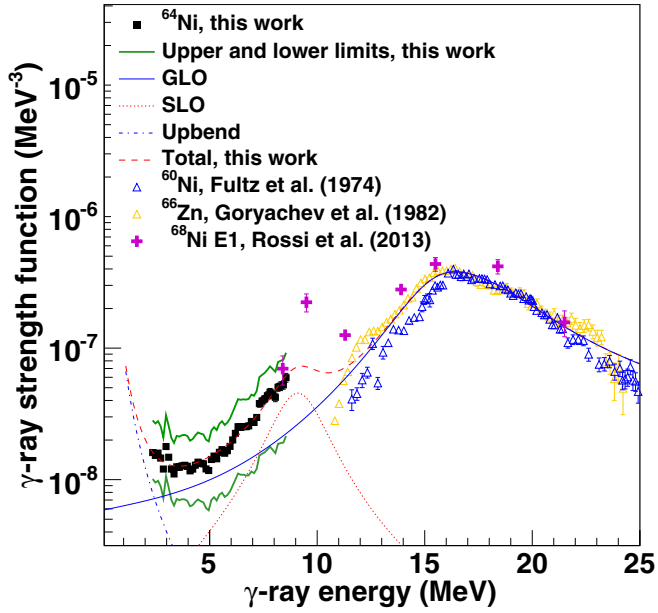

FIG. 3. The γ-ray-strength function of ^{64}Ni (black squares), together with its upper and lower limits (solid green lines). The GDR datasets for ^{60}Ni [51] and ^{66}Zn [52] used for normalization are also shown. The estimated GDR strength for the ^{64}Ni data has been included, together with the models used to reproduce the resonancelike structures. The estimated total strength for the ^{64}Ni data is depicted as a red dashed line. Data on the GDR for ^{68}Ni are also shown [54].

possible resonance, a standard Lorentzian curve (SLO) [39] was fitted to the experimental data and a term f^{SLO} was added to the estimated GDR strength,

$$f^{\mathrm{SLO}}(E_\gamma) = \frac{1}{3\pi^2\hbar^2c^2}\frac{\sigma_{\mathrm{SLO}}E_\gamma\Gamma_{\mathrm{SLO}}^2}{\left(E_\gamma^2 - E_{\mathrm{SLO}}^2\right)^2 + E_\gamma^2\Gamma_{\mathrm{SLO}}^2}, \tag{22}$$

where σ_{SLO}, E_{SLO}, and Γ_{SLO} are the peak cross section, energy centroid, and resonance width parameters for the SLO.

The set of parameters σ_{SLO}, E_{SLO}, Γ_{SLO} in Eq. (22) and C and η in Eq. (21) were then obtained from the fitting to the ^{64}Ni data. The resulting total γ strength, $f^{\mathrm{total}} = f_{E1}^{\mathrm{GLO}} + f^{\mathrm{SLO}} + f^{\mathrm{upb}}$ for the ^{64}Ni data is shown as a red dashed line in Fig. 3. Several fittings were performed for different normalizations of the γ strength of ^{64}Ni, allowing for the estimation of the uncertainties in the γ-strength parameters. The estimated f^{SLO} term is the minimum required to reproduce our data above $E_\gamma \approx 7$ MeV, to obtain a conservative estimate of the additional γ strength with respect to the GLO term. It must be noted that the inclusion of a SLO centered at $E_\gamma \approx 9.2$ MeV is also necessary to reproduce the estimated upper limit for the ^{64}Ni γ strength, while the estimated lower limit can be reproduced without adding a SLO.

The parameters in f^{total} were obtained for γ-strength functions corresponding to the level densities from normalizations 1 and 2, described in Sec. III A. The resulting γ-strength function from normalization 2 was very similar and within the error bars of the γ strength from normalization 1 and it has therefore not been included on Fig. 3. The final parameters for

TABLE IV. Parameters used for the γ-strength function models of ^{64}Ni.

$E_{E1,1}$ (MeV)	$\sigma_{E1,1}$ (mb)	$\Gamma_{E1,1}$ (MeV)	$E_{E1,2}$ (MeV)	$\sigma_{E1,2}$ (mb)	$\Gamma_{E1,2}$ (MeV)	T_f (MeV)	$E_{\rm SLO}$ (MeV)	$\sigma_{\rm SLO}$ (mb)	$\Gamma_{\rm SLO}$ (MeV)	C (MeV^{-3})	η (MeV^{-1})
16.6 ± 0.8	62.4 ± 20.0	4.8 ± 2.0	19.0 ± 0.9	31.2 ± 10.0	6.6 ± 2.6	1.20 ± 0.50	9.2	4.8 ± 4.8	2.7 ± 0.5	1.0 ± 0.7	2.8 ± 0.4

the γ-strength function from normalization 1 are summarized in Table IV. The parameters for normalization 2 are close in value to those for normalization 1 and well contained within their estimated uncertainties. Therefore, from now on the discussion will be based on the results from normalization 1.

IV. COMPARISON WITH OTHER DATA AND CALCULATION OF THE ^{63}Ni(n,γ) CROSS SECTION AND REACTION RATE

The extracted nuclear level density from Sec. III was compared to the data deduced from particle-evaporation measurements at $E_x > 5.5$ MeV [55]. The comparison, presented in Fig. 4, shows a good agreement between the results from the present work and the data from Ref. [55] in the overlapping region. Moreover, the estimated temperature parameter from this work $T = 1.13(13)$ MeV is in good agreement with the value from Ref. [55], $T_{\rm Ref.} = 1.163$ MeV. In addition, the extracted level density presents some steplike structures at $E_x \simeq 3.6$ MeV, $E_x \simeq 5.8$ MeV, and $E_x \simeq 6.7$ MeV, which could be related to the breaking of nucleon pairs and/or shell effects. As the excitation energy increases and more nucleon pairs are broken, the structures are "smeared out" and the level density becomes smoother, as seen in the data from Ref. [55] at $E_x > 8.5$ MeV.

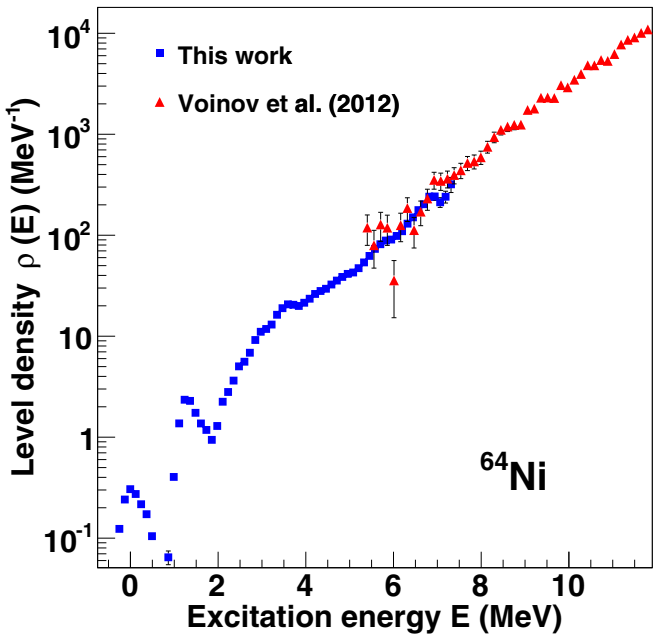

FIG. 4. Experimental nuclear level density for ^{64}Ni from the present work (as obtained in normalization 1) compared to the level density from Ref. [55].

Regarding the γ-strength function, the first clear observation is the presence of additional strength with respect to the tail of the GDR strength. Unfortunately, whether this strength is of $E1$ or $M1$ character could not be determined in the present work. The most obvious component of this additional strength is the observed low-energy enhancement which is comparable to the upbend seen in other light and medium-mass nuclei. Figure 5 shows the comparison of the results for ^{64}Ni with those for ^{56}Fe [13], ^{76}Ge [56], and ^{94}Mo [12]. The observed upbend in ^{64}Ni is similar to the one seen in ^{56}Fe, while the γ-strength function of ^{76}Ge and ^{94}Mo look different from the results for ^{64}Ni and more similar to each other. In the case of ^{60}Ni, the results from Ref. [21] strongly indicate that the upbend is mainly attributable to $M1$ transitions. However, ^{60}Ni is a special case with only positive-parity states below excitation energies of $\simeq$4.5 MeV, contributing to the enhancement of $M1$ transitions. For the present work, in contrast, even though ^{64}Ni has only positive-parity states below $E_x \simeq 3$ MeV, the initial states in the decay chosen for the Oslo method are at $E_x \simeq 5.82$–9.66 MeV. At these excitation energies, both positive- and negative-parity states are present. Therefore, both $E1$ and $M1$ transitions could, in principle, be contributing to the observed low-energy enhancement in ^{64}Ni.

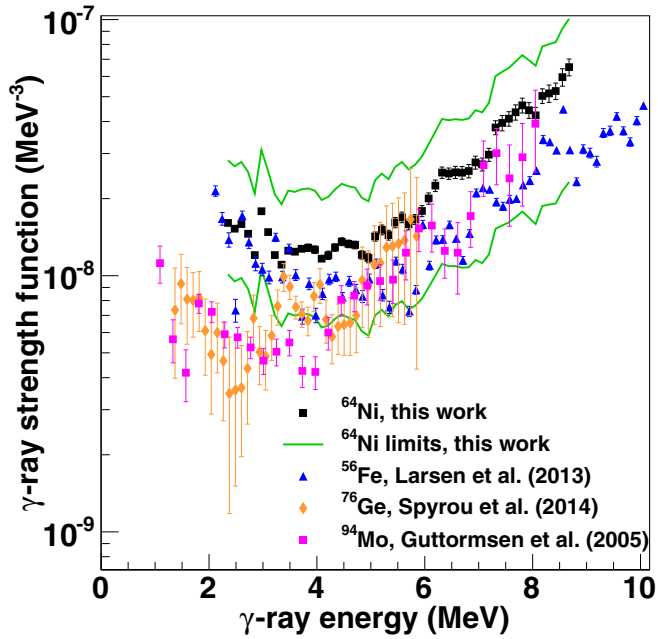

FIG. 5. The γ-strength function of ^{64}Ni obtained in the present work compared to the γ strength of ^{56}Fe [13], ^{76}Ge [56], and ^{94}Mo [12]. All these nuclei present a low-energy enhancement or upbend in the γ-strength function. In addition, the upper and lower limits for the γ-strength function estimated in this work have been depicted as green solid lines.

In addition, the data indicate the presence of additional strength with respect to the GDR which can be reproduced by the inclusion of a SLO centered at $E_\gamma \simeq 9.2$ MeV. Although the lower limit for the γ-strength function can be reproduced without such a structure, its inclusion is necessary to reproduce our estimated γ strength (black squares in Figs. 3 and 5) as well as the upper limit. If a resonance was truly present at $E_\gamma \simeq 9.2$ MeV, it would be of great interest to determine whether it is of $E1$ or $M1$ character. If found to be of $E1$ character, it would very probably be the result of a pygmy resonance, often described as owing to the oscillation of the neutron skin with respect to a $N \approx Z$ core [57,58]. If so, the measured resonance would be in agreement with the observations for ^{68}Ni, which also presents an $E1$ pygmy resonance at $E_\gamma \simeq 9.6$ MeV that has been interpreted as a possible neutron-skin oscillation [54,59]. However, this possible resonance at $E_\gamma \simeq 9.2$ MeV could as well be of $M1$ character, being in that case probably owing to $M1$ spin-flip transitions. This would be in agreement with the results for ^{60}Ni, which indicate accumulations of $M1$ excited spin-1 states near $E_x = 8$ MeV and $E_x = 9$ MeV, identified as isoscalar and isovector $M1$ resonances dominated by proton and neutron $f_{7/2} \longrightarrow f_{5/2}$ spin-flip excitations [60]. In addition, results from Ref. [61] also indicate the presence of resonances with a significant $M1$ component at $E_\gamma \approx 9$–14 MeV in ^{58,60,62}Ni. Finally, for the case of ^{64}Ni, with mass in between ^{58,60,62}Ni and ^{68}Ni, one should also consider the possibility that the observed additional strength might not be solely of $E1$ or $M1$ nature, but a mixture of both.

As a final remark regarding the γ-strength function, the presence of a sharp structure at $E_\gamma \approx 3$ MeV is noted. This structure most likely has its origin in leftover secondary transitions present in the first-generation matrix, which are seen as a ridge centered at $E_\gamma \approx 3$ MeV in Fig. 1(c). However, it has no impact on the overall shape of the γ-strength function.

The normalized nuclear level density and γ-strength function of ^{64}Ni have been used to calculate the ^{63}Ni$(n,\gamma)^{64}$Ni cross section and reaction rate with the code TALYS [31] for simulation of nuclear reactions. The resulting cross section, depicted in Fig. 6, has been compared with measurements from Refs. [28,29]. The figure also shows the estimated upper and lower limits for the cross section when the uncertainties in the γ-strength function and the nuclear level density are included. The highest contribution to the uncertainty in the obtained cross section is attributable to the high uncertainty in the absolute normalization of the γ-strength function, while other systematic errors, such as those related to the parity asymmetry or the model for the spin cutoff parameter have a much smaller effect. The parameters applied in the TALYS calculations are listed in Table V. Notice that the lower limit

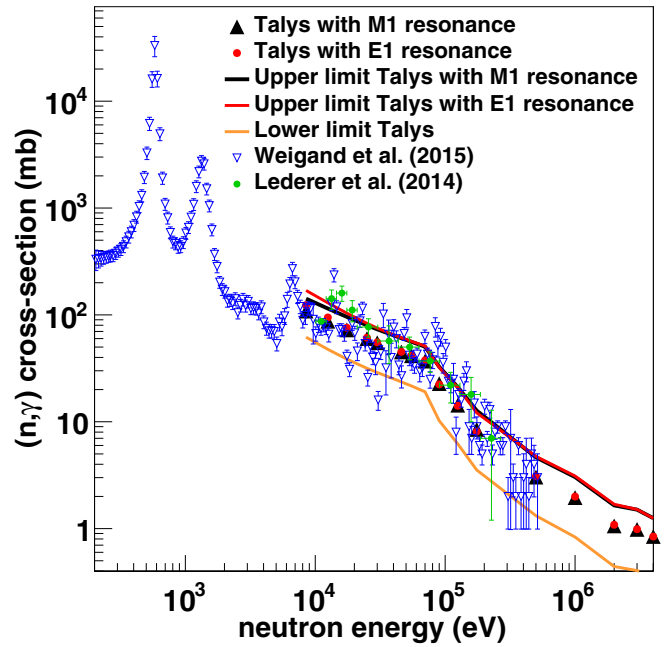

FIG. 6. The ^{63}Ni$(n,\gamma)^{64}$Ni cross section from Refs. [29] and [28] compared to the one calculated with TALYS using the level density and γ-strength function obtained in this work. The lower and upper limits for the estimated cross section associated with the systematic errors are depicted as solid lines. For the cases in which the ^{64}Ni γ strength presents a resonancelike structure at $E_\gamma \approx 9.2$ MeV, the calculations have been performed assuming a resonance of purely $M1$ character (black) and purely $E1$ character (red).

for the cross section corresponds to the lower limit for the γ-strength function of ^{64}Ni, reproduced without the inclusion of a resonance at $E_\gamma \approx 9.2$ MeV. In contrast, the expected and upper limits for the cross section correspond to the presence of a resonancelike structure centered at $E_\gamma \approx 9.2$ MeV. The TALYS calculations for these cases have been performed considering the additional strength at $E_\gamma \approx 9.2$ MeV to be purely of $M1$ character (black) and purely of $E1$ character (red).

As seen in Fig. 6, the results from this work are in excellent agreement with those of Ref. [29]. A good agreement is also seen with the data from Ref. [28]. Below ≈10 keV the data from Ref. [28] indicate the presence of strong neutron resonances, which cannot easily be reproduced with TALYS simulations based on the Hauser-Feshbach approach [31,62]. The cross sections obtained when additional $E1$ strength at $E_\gamma \approx 9.2$ MeV is included are higher than those resulting from the inclusion of purely $M1$ strength, leading to a better agreement with the results from Ref. [29].

TABLE V. Parameters used for the input models in the TALYS calculations. The spin distribution is given by the BSFG model in all cases.

	$\rho(S_n)$ (MeV^{-1})	T (MeV)	E_0 (MeV)	$E_{E1,1}$ (MeV)	$\sigma_{E1,1}$ (mb)	$\Gamma_{E1,1}$ (MeV)	$E_{E1,2}$ (MeV)	$\sigma_{E1,2}$ (mb)	$\Gamma_{E1,2}$ (MeV)	T_f (MeV)	$E_{\rm SLO}$ (MeV)	$\sigma_{\rm SLO}$ (mb)	$\Gamma_{\rm SLO}$ (MeV)	C (MeV^{-3})	η (MeV^{-1})
Middle value	2620	1.13	0.63	16.6	62.4	4.8	19.0	31.2	6.6	1.20	9.2	4.8	2.7	1.0	2.8
Lower limit	1730	1.2	0.49	16.6	57.4	5.3	19.0	28.2	7.0	0.94	–	–	–	0.6	2.9
Upper limit	3510	1.1	1.50	16.6	66.4	4.2	19.0	34.0	6.4	1.62	9.2	7.8	2.7	1.3	2.5

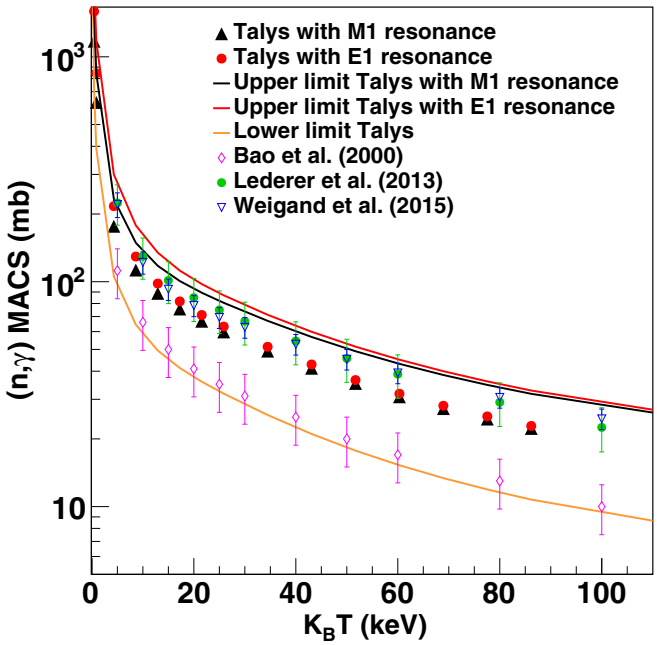

FIG. 7. MACS obtained with TALYS using the level density and γ-strength function from this work. The results are presented as a function of K_BT, where T is the temperature and K_B is the Boltzmann constant. Theoretical values from Ref. [63] and estimates based on measurements from Ref. [30] and [28] are included for comparison. The lower and upper limits estimated in this work are depicted as solid lines. For the cases in which the ^{64}Ni γ strength presents a resonancelike structure at $E_\gamma \approx 9.2$ MeV, the calculations have been performed assuming a resonance of purely $M1$ character (black) and purely $E1$ character (red).

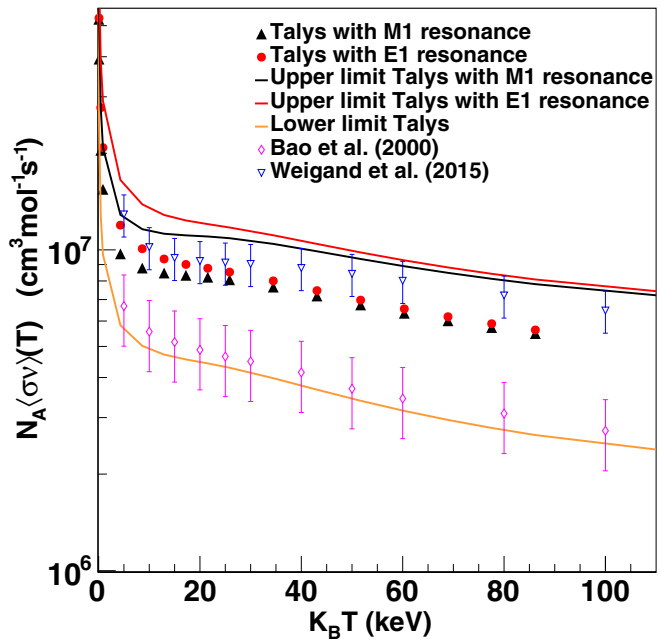

FIG. 8. The ^{63}Ni$(n,\gamma)^{64}$Ni reaction rate obtained with TALYS as a function of temperature T, where K_B is the Boltzmann constant. The results from this work have been compared to theoretical values from Ref. [63] and estimates based on measurements from Ref. [28]. The lower and upper limits from this work are depicted as solid lines. For the cases in which the ^{64}Ni γ strength presents a resonancelike structure at $E_\gamma \approx 9.2$ MeV, the calculations have been performed assuming a resonance of purely $M1$ character (black) and purely $E1$ character (red).

The TALYS calculations presented in this work correspond to normalization 1 of the nuclear level density, described in Sec. III A and results for the γ-strength function shown in Figs. 3 and 5. The applied spin distribution is therefore given by the BSFG model in all cases. The calculations were tested for normalization 2 of the nuclear level density and found to be within the estimates for normalization 1.

The Maxwellian averaged cross section (MACS) has also been obtained with TALYS and compared with theoretical calculations from Ref. [63] and estimates based on measurements from Refs. [30] and [28]. As seen in Fig. 7, the theoretical values from Ref. [63] are in agreement with the lower limit obtained in this work, while the results from Ref. [30] are in very good agreement with our expected values. The results from Ref. [28] are well contained within the upper half of our error band, showing a better agreement with our estimates for the case in which the possible additional strength at $E_\gamma \approx 9.2$ MeV is considered of $E1$ character.

Finally, Fig. 8 shows the ^{63}Ni$(n,\gamma)^{64}$Ni reaction rates obtained in this work together with the theoretical predictions from Ref. [63] and the estimates based on measurements from Ref. [28]. An uncertainty of 25% has been included in the values from Ref. [63] based on their standard uncertainties for the MACS, while a value of 15% uncertainty has been included in the data from Ref. [28], based on their uncertainties for the (n,γ) cross section and MACS. The estimates from this work are higher than those from Ref. [63] by a factor of ≈2–3, although the lower limit for our result agrees with those from Ref. [63]. The more recent results from Ref. [28] are again well contained within the upper half of our estimated error band, with a better agreement for the calculations in which the possible resonance at $E_\gamma \approx 9.2$ MeV is considered of $E1$ character. Assuming $M1$ character for the possible resonance, lower rates are obtained, the difference being more obvious at energies below ≈30 keV.

V. SUMMARY AND OUTLOOK

The level density and γ-ray-strength function of ^{64}Ni have been extracted from particle-γ coincidence measurements by means of the Oslo method. The normalization procedure has been applied using two different spin cutoff parameters, leading to similar results that are within each other's systematic uncertainties. The effect of parity asymmetry has also been estimated and found to be of less significance with respect to the systematic errors associated with the normalization procedure. The level density of ^{64}Ni is in good agreement with the known levels at low excitation energy as well as with data deduced from particle-evaporation measurements at excitation energies above ≈5.5 MeV. In addition, some steplike structures are seen in the level density, which could be related to the breaking of nucleon pairs and shell effects.

The γ-strength function displays additional strength with respect to the tail of the GDR given by the GLO model. The data clearly suggest the presence of an enhancement of the γ strength below 3 MeV. This enhancement or upbend has also been seen in ^{60}Ni from two-step cascade measurements, with strong indications of being mainly attributable to $M1$ transitions. In addition, a resonancelike structure might be present at $E_\gamma \approx 9.2$ MeV. If such a resonance was present, it could correspond to spin-flip transitions if found to be mainly of $M1$ character. However, if found to be mostly of $E1$ nature, it could be a pygmy dipole resonance. Future experiments to determine the electromagnetic character of the observed upbend and possible resonance in ^{64}Ni are therefore highly desirable.

Finally, the extracted nuclear level density and γ strength of ^{64}Ni have been used as input for the code TALYS to estimate the ^{63}Ni$(n,\gamma)^{64}$Ni cross section and reaction rate. The results from the present work are in good agreement with available measurements as well as with the theoretical predictions from other references.

ACKNOWLEDGMENTS

We would like to thank INFN Laboratory Nazionali di Legnaro for providing the ^{64}Ni target. We are also grateful for the financial support received from the Research Council of Norway (NFR). A.C.L. acknowledges support by the NFR under project Grant No. 205528 and the ERC-STG-2014 under Grant Agreement No. 637686. S.S. acknowledges financial support by the NFR under Project Grant No. 210007 and G.M.T. acknowledges support by the NFR under Project Grant No. 222287. Finally, we would like to specially thank J. C. Müller, A. Semchenkov, and J. Wikne for providing the beam for our experiment.

[1] G. A. Bartholomew *et al.*, in *Advances in Nuclear Physics*, edited by M. Baranger and E. Vogt (Plenum, New York, 1973), Vol. 7, p. 229.
[2] T. Ericson, Nucl. Phys. **11**, 481 (1959).
[3] T. Ericson and V. Struzinsky, Nucl. Phys. **8**, 284 (1958); **9**, 689 (1958/1959).
[4] E. Melby, L. Bergholt, M. Guttormsen, M. Hjorth-Jensen, F. Ingebretsen, S. Messelt, J. Rekstad, A. Schiller, S. Siem, and S. W. Ødegård, Phys. Rev. Lett. **83**, 3150 (1999).
[5] B. L. Berman and S. C. Fultz, Rev. Mod. Phys. **47**, 713 (1975).
[6] D. Savran, T. Aumann, and A. Zilges, Prog. Part. Nucl. Phys. **70**, 210 (2013).
[7] M. Guttormsen, T. S. Tveter, L. Bergholt, F. Ingebretsen, and J. Rekstad, Nucl. Instrum. Methods Phys. Res. A **374**, 371 (1996).
[8] M. Guttormsen, T. Ramsøy, and J. Rekstad, Nucl. Instrum. Methods Phys. Res. A **255**, 518 (1987).
[9] A. Schiller, L. Bergholt, M. Guttormsen, E. Melby, J. Rekstad, and S. Siem, Nucl. Instrum. Methods Phys. Res. A **447**, 498 (2000).
[10] A. C. Larsen, M. Guttormsen, M. Krtička, E. Běták, A. Bürger, A. Görgen, H. T. Nyhus, J. Rekstad, A. Schiller, S. Siem, H. K. Toft, G. M. Tveten, A. V. Voinov, and K. Wikan, Phys. Rev. C **83**, 034315 (2011).
[11] A. Voinov, E. Algin, U. Agvaanluvsan, T. Belgya, R. Chankova, M. Guttormsen, G. E. Mitchell, J. Rekstad, A. Schiller, and S. Siem, Phys. Rev. Lett. **93**, 142504 (2004).
[12] M. Guttormsen, R. Chankova, U. Agvaanluvsan, E. Algin, L. A. Bernstein, F. Ingebretsen, T. Lönnroth, S. Messelt, G. E. Mitchell, J. Rekstad, A. Schiller, S. Siem, A. C. Sunde, A. Voinov, and S. Ødegård, Phys. Rev. C **71**, 044307 (2005).
[13] A. C. Larsen, N. Blasi, A. Bracco, F. Camera, T. K. Eriksen, A. Görgen, M. Guttormsen, T. W. Hagen, S. Leoni, B. Million, H. T. Nyhus, T. Renstrøm, S. J. Rose, I. E. Ruud, S. Siem, T. Tornyi, G. M. Tveten, A. V. Voinov, and M. Wiedeking, Phys. Rev. Lett. **111**, 242504 (2013).
[14] A. C. Larsen, I. E. Ruud, A. Bürger, S. Goriely, M. Guttormsen, A. Görgen, T. W. Hagen, S. Harissopulos, H. T. Nyhus, T. Renstrøm, A. Schiller, S. Siem, G. M. Tveten, A. Voinov, and M. Wiedeking, Phys. Rev. C. **89**, 014319 (2014).
[15] A. C. Larsen, M. Guttormsen, R. Chankova, F. Ingebretsen, T. Lönnroth, S. Messelt, J. Rekstad, A. Schiller, S. Siem, N. U. H. Syed, and A. Voinov, Phys. Rev. C **76**, 044303 (2007).
[16] A. Bürger *et al.*, Phys. Rev. C **85**, 064328 (2012).
[17] A. C. Larsen, R. Chankova, M. Guttormsen, F. Ingebretsen, S. Messelt, J. Rekstad, S. Siem, N. U. H. Syed, S. W. Ødegård, T. Lonnroth, A. Schiller, and A. Voinov, Phys. Rev. C **73**, 064301 (2006).
[18] B. V. Kheswa, M. Wiedeking, F. Giacoppo, S. Goriely, M. Guttormsen, A. C. Larsen, F. L. Bello Garrote, T. K. Eriksen, A. Görgen, T. W. Hagen, P. E. Koehler, M. Klintefjord, H. T. Nyhus, P. Papka, T. Renstrøm, S. Rose, E. Sahin, S. Siem, and T. G. Tornyi, Phys. Lett. B **744**, 268 (2015).
[19] A. Simon, M. Guttormsen, A. C. Larsen, C. W. Beausang, P. Humby, J. T. Burke, R. J. Casperson, R. O. Hughes, T. J. Ross, J. M. Allmond, R. Chyzh, M. Dag, J. Koglin, E. McCleskey, M. McCleskey, S. Ota, and A. Saastamoinen, Phys. Rev. C **93**, 034303 (2016).
[20] M. Wiedeking, L. A. Bernstein, M. Krtička, D. L. Bleuel, J. M. Allmond, M. S. Basunia, J. T. Burke, P. Fallon, R. B. Firestone, B. L. Goldblum, R. Hatarik, P. T. Lake, I.-Y. Lee, S. R. Lesher, S. Paschalis, M. Petri, L. Phair, and N. D. Scielzo, Phys. Rev. Lett. **108**, 162503 (2012).
[21] A. Voinov, S. M. Grimes, C. R. Brune, M. Guttormsen, A. C. Larsen, T. N. Massey, A. Schiller, and S. Siem, Phys. Rev. C **81**, 024319 (2010).
[22] E. Litvinova and N. Belov, Phys. Rev. C **88**, 031302(R) (2013).
[23] R. Schwengner, S. Frauendorf, and A. C. Larsen, Phys. Rev. Lett. **111**, 232504 (2013).
[24] B. A. Brown and A. C. Larsen, Phys. Rev. Lett. **113**, 252502 (2014).
[25] A. C. Larsen and S. Goriely, Phys. Rev. C **82**, 014318 (2010).
[26] I. Daoutidis and S. Goriely, Phys. Rev. C **86**, 034328 (2012).
[27] F. Käppeler, R. Gallino, S. Bisterzo, and W. Aoki, Rev. Mod. Phys. **83**, 157 (2011).
[28] M. Weigand, T. A. Bredeweg, A. Couture, K. Gobel, T. Heftrich, M. Jandel, F. Kappeler, C. Lederer, N. Kivel, G. Korschinek, M. Krticka, J. M. O'Donnell, J. Ostermoller, R. Plag, R. Reifarth, D. Schumann, J. L. Ullmann, and A. Wallner, Phys. Rev. C **92**, 045810 (2015).

[29] C. Lederer *et al.*, Phys. Rev. C **89**, 025810 (2014).
[30] C. Lederer *et al.*, Phys. Rev. Lett. **110**, 022501 (2013).
[31] A. J. Koning, S. Hilaire, and M. C. Duijvestijn, TALYS-1.6, software for simulation of nuclear reactions, http://www.talys.eu/home/; TALYS-1.0, *Proceedings of the International Conference on Nuclear Data for Science and Technology-ND2007, April 22–27, 2007, Nice, France*, edited by O. Bersillon, F. Gunsing, E. Bauge, R. Jacqmin, and S. Leray (EDP Sciences, Les Ulis, France, 2008), pp. 211–214; A. J. Koning and D. Rochman, Nucl. Data Sheets **113**, 2841 (2012).
[32] M. Guttormsen, A. Bürger, T. E. Hansen, and N. Lietaer, Nucl. Instrum. Methods Phys. Res. A **648**, 168 (2011).
[33] M. Guttormsen, A. Ataç, G. Løvhøiden, S. Messelt, T. Ramsøy, J. Rekstad, T. F. Thorsteinsen, T. S. Tveter, and Z. Zelazny, Phys. Scr., T **32**, 54 (1990).
[34] A. Bohr and B. Mottelson, *Nuclear Structure* (W. A. Benjamin, New York, 1969), Vol. I.
[35] D. M. Brink, P.h.D. thesis, Oxford University, 1955.
[36] A. Schiller and M. Thoennessen, At. Data Nucl. Data Tables **93**, 549 (2007).
[37] M. Guttormsen, A. C. Larsen, A. Görgen, T. Renstrøm, S. Siem, T. G. Tornyi, and G. M. Tveten, Phys. Rev. Lett. **116**, 012502 (2016).
[38] Data extracted using the NNDC On-Line Data Service from the ENSDF database, 2015, http://www.nndc.bnl.gov/ensdf/.
[39] T. Belgya *et al.*, *Handbook for Calculations of Nuclear Reaction Data, RIPL-2*, IAEA-TECDOC-1506, Vienna, 2006.
[40] J. Kopecky and M. Uhl, Phys. Rev. C **41**, 1941 (1990).
[41] R. Capote *et al.*, *Reference Input Parameter Library*, RIPL-3; available online at http://www-nds.iaea.org/RIPL-3/.
[42] R. Capote *et al.*, Nucl. Data Sheets **110**, 3107 (2009).
[43] T. von Egidy and D. Bucurescu, Phys. Rev. C **80**, 054310 (2009).
[44] T. von Egidy and D. Bucurescu, Phys. Rev. C **72**, 044311 (2005); **73**, 049901(E) (2006).
[45] A. Gilbert and A. G. W. Cameron, Can. J. Phys. **43**, 1446 (1965).
[46] A. Schiller, E. Algin, L. A. Bernstein, P. E. Garrett, M. Guttormsen, M. Hjorth-Jensen, C. W. Johnson, G. E. Mitchell, J. Rekstad, S. Siem, A. Voinov, and W. Younes, Phys. Rev. C. **68**, 054326 (2003).
[47] Y. Kalmykov, C. Ozen, K. Langanke, G. Martínez-Pinedo, P. von Neumann-Cosel, and A. Richter, Phys. Rev. Lett. **99**, 202502 (2007).
[48] U. Agvaanluvsan, G. E. Mitchell, J. F. Shriner, Jr., and M. Pato, Phys. Rev. C **67**, 064608 (2003).
[49] D. Mocelj, T. Rauscher, G. Martínez-Pinedo, K. Langanke, L. Pacearescu, A. Faessler, F. K. Thielemann, and Y. Alhassid, Phys. Rev. C **75**, 045805 (2007).
[50] S. Goriely, S. Hilaire, and A. J. Koning, Phys. Rev. C **78**, 064307 (2008).
[51] A. M. Goryachev, Vopr. Teor. Yadernoy Fiz. **8**, 121 (1982).
[52] S. C. Fultz, R. A. Alvarez, B. L. Berman, and P. Meyer, Phys. Rev. C **10**, 608 (1974).
[53] W. Thomas, Naturwissenschaften **13**, 627 (1925); W. Kuhn, Z. Phys. **33**, 408 (1925); F. Reiche and W. Thomas, *ibid.* **34**, 510 (1925).
[54] D. M. Rossi *et al.*, Phys. Rev. Lett. **111**, 242503 (2013).
[55] A. Voinov, S. M. Grimes, C. R. Brune, T. Massey, and A. Schiller, EPJ Web Conf. **21**, 05001 (2012); A. Voinov (private communication).
[56] A. Spyrou, S. N. Liddick, A. C. Larsen, M. Guttormsen, K. Cooper, A. C. Dombos, D. J. Morrissey, F. Naqvi, G. Perdikakis, S. J. Quinn, T. Renstrøm, J. A. Rodriguez, A. Simon, C. S. Sumithrarachchi, and R. G. T. Zegers, Phys. Rev. Lett. **113**, 232502 (2014).
[57] Y. Suzuki, K. Ikeda, and H. Sato, Prog. Theor. Phys. **83**, 180 (1990).
[58] P. Van Isacker, M. A. Nagarajan, and D. D. Warner, Phys. Rev. C **45**, R13 (1992).
[59] O. Wieland *et al.*, Phys. Rev. Lett. **102**, 092502 (2009).
[60] M. Scheck, V. Yu. Ponomarev, M. Fritzsche, J. Joubert, T. Aumann, J. Beller, J. Isaak, J. H. Kelley, E. Kwan, N. Pietralla, R. Raut, C. Romig, G. Rusev, D. Savran, L. Schorrenberger, K. Sonnabend, A. P. Tonchev, W. Tornow, H. R. Weller, A. Zilges, and M. Zweidinger, Phys. Rev. C **88**, 044304 (2013).
[61] C. Djalali, N. Marty, M. Morlet, A. Willis, J. C. Jourdain, N. Anantaraman, G. M. Crawley, A. Galonsky, and P. Kitching, Nucl. Phys. A **388**, 1 (1982).
[62] W. Hauser and H. Feshbach, Phys. Rev. **87**, 366 (1952).
[63] Z. Y. Bao, H. Beer, F. Käppeler, F. Voss, K. Wisshak, and T. Rauscher, At. Data Nucl. Data Tables **76**, 70 (2000); I. Dillmann, M. Heil, F. Käppeler, R. Plag, T. Rauscher, and F. K. Thielemann, AIP Conf. Proc. **819**, 123; online at http://www.kadonis.org.